

Original scientific paper

BENEFICIAL EFFECT OF CU CONTENT AND AUSTEMPERING PARAMETERS ON THE HARDNESS AND CORROSION PROPERTIES OF AUSTEMPERED DUCTILE IRON (ADI)

Ladislav Vrsalović¹, Nikša Čatipović², Senka Gudić¹, Stjepan Kožuh³

¹University of Split, Faculty of Chemistry and Technology, Split, Croatia

²University of Split, Faculty of Electrical Engineering,
Mechanical Engineering and Naval Architecture, Split, Croatia

³University of Zagreb, Faculty of Metallurgy, Sisak, Croatia

ORCID iDs: Ladislav Vrsalović
Nikša Čatipović
Senka Gudić
Stjepan Kožuh

<https://orcid.org/0000-0001-6111-5475>
<https://orcid.org/0000-0002-5031-0766>
<https://orcid.org/0000-0001-5390-5215>
<https://orcid.org/0000-0003-2536-2713>

Abstract. *The effect of copper content (0.031 wt.% Cu, 0.32 wt.% Cu, 0.51 wt.% Cu and 0.91 wt.% Cu) on the hardness and corrosion properties of ADI was investigated. Samples austenitization were carried out at 850°C for 60 min followed by its austempering at temperatures from 250°C to 420°C for different time (30 to 60 min) in 50% (KNO₃ + NaNO₃) salt bath. It was concluded that hardness rises with copper content but decreases with higher austempering temperatures and times. The corrosion properties of the samples with minimum and maximum Cu content were investigated by electrochemical methods in 0.5 M NaCl solution. Samples with a higher copper content have shown higher values of polarization resistance (R_p) and lower values of corrosion current (i_{corr}). After polarization measurements, corroded surfaces were analyzed with SEM/EDS analysis.*

Key Words: *Copper Content, ADI, Hardness, Corrosion Properties, SEM, EDS*

1. INTRODUCTION

Ductile iron (DI) is a high carbon cast ferrous material with a composition similar to grey iron, in which carbon is present in the form of spheroids graphite instead of conventional flake or plate form, which is characteristics of grey iron [1, 2]. It is significantly used in different industrial applications, including construction, mining, agriculture, automotive parts and machines, tubes, etc. [3-5]. The reason for its common use lies in its advantages over steel castings and grey iron castings. Appropriate heat treatment and alloying leads to improve

Received: January 06, 2022 / Accepted April 03, 2022

Corresponding author: Nikša Čatipović

Faculty of Electrical Engineering, Mechanical Engineering and Naval Architecture, Ruđera Boškovića 32, 21100 Split, Croatia

E-mail: ncatipov@fesb.hr

the strength, hardness, and wear resistance of DI. Austempering treatment can achieve the transformation of ductile iron into alloy with the microstructure of acicular ferrite and retained austenite [6]. Austempered ductile iron (ADI) was commercialized during the 1970s. Its application steadily grew due to its high tensile strength, good fatigue resistance under dynamic loading conditions, abrasion resistance and toughness [5-9]. The benefits of using ADI material are reflected in its good mechanical properties, such as good vibration properties, lighter weight than other structural materials, and uniform castability. Investigations of mechanical properties of DI and ADI have been in the focus of many published studies, but the related studies on its corrosion properties are significantly less published. Corrosion susceptibility of DI lies in the fact that graphite is nobler than the iron matrix, and it acts as a cathode when the DI surface is exposed to the corrosive environment [2]. The presence of alloying elements, like copper, nickel and molybdenum, leads to microstructural changes in DI, which affect its mechanical and electrochemical behavior [6, 10-12]. Nickel addition increased pearlite content, decreased the nodule count, and reduced the graphitic corrosion of ductile iron [10]. An increase in molybdenum content leads to a rise in the quantity of retained austenite and carbide. At the same time, the acicular ferrite becomes finer, which leads to increased wear and corrosion resistance [6]. Higher silicon content in this material increased its susceptibility to localized corrosion in chloride media [13]. The increase in austenite temperature and processing time decreases its corrosion rate [13,14]. Also, surface treatments, like laser surface alloying, plasma oxidation treatment and plasma nitriding increase the corrosion resistance of ductile iron [15,16].

This paper deals with investigating the influence of Cu content on hardness and corrosion properties of the DI and ADI in 0.5 M NaCl solution. The as-cast specimens of DI were first austenitized at 850°C for 60 min and then austempered in 50% NaNO₃- 50% KNO₃ salt bath at temperatures from 250°C to 420°C for 30 to 60 min to produce ADI.

2. EXPERIMENTAL PROCEDURE

The chemical composition of the ductile iron samples is shown in Table 1.

Table 1 Chemical composition of ductile iron samples

Alloy	C(%)	Si(%)	Mn(%)	Cu(%)	S(%)	P(%)	Cr(%)	V(%)
	3.63	2.61	0.135	0.031	0.0035	0.022	0.005	0.004
1.	Ni(%)	Mo(%)	Al(%)	Ti(%)	Sn(%)	W(%)	Mg(%)	
	0.085	0.003	0.017	0.013	0.033	0.017	0.041	
Alloy	C(%)	Si(%)	Mn(%)	Cu(%)	S(%)	P(%)	Cr(%)	V(%)
	3.63	2.61	0.135	0.32	0.0035	0.022	0.005	0.004
2.	Ni(%)	Mo(%)	Al(%)	Ti(%)	Sn(%)	W(%)	Mg(%)	
	0.085	0.003	0.017	0.013	0.033	0.017	0.041	
Alloy	C(%)	Si(%)	Mn(%)	Cu(%)	S(%)	P(%)	Cr(%)	V(%)
	3.63	2.61	0.135	0.51	0.0035	0.022	0.005	0.004
3.	Ni(%)	Mo(%)	Al(%)	Ti(%)	Sn(%)	W(%)	Mg(%)	
	0.085	0.003	0.017	0.013	0.033	0.017	0.041	
Alloy	C(%)	Si(%)	Mn(%)	Cu(%)	S(%)	P(%)	Cr(%)	V(%)
	3.63	2.61	0.135	0.91	0.0035	0.022	0.005	0.004
4.	Ni(%)	Mo(%)	Al(%)	Ti(%)	Sn(%)	W(%)	Mg(%)	
	0.085	0.003	0.017	0.013	0.033	0.017	0.041	

The first step was to heat treat ductile iron samples to produce ADI samples. All samples were austenitized at the same temperature of 850°C for the same time of 60 min. After austenitization, austempering was performed according to the experimental plan, Table 2. The austempering temperature was changed between 250°C and 420°C, and austempering time was varied between 30 min and 60 min. Planning of experiments in respect to input parameters was performed by Design Expert software. The cubic model was selected for Response Surface Method (RSM) study type with D-optimal initial design [17].

Table 2 Experimental plan according to Design Expert software

Sample ID	Wt. % Cu	Austempering temperature, [°C]	Austempering time, [min]
10	0.32 %	335	45
11		420	47
12		250	42
13		320	60
14		320	60
15		349	30
16		349	30
20	0.91 %	420	60
21		420	30
22		420	60
23		299	30
24		250	51
25		250	51
30	0.031 %	420	30
31		335	60
32		335	45
33		255	36
34		420	60
35		250	60
40		0.51 %	420
41	335		39
42	420		60
43	250		30
44	250		60
45	420		30

Vickers hardness HV10 was measured at an applied load of 98 N using a universal hardness machine according to ISO standard 6507-1:2005.

The electrodes for the electrochemical measurements were made from DI and ADI cylindrical samples $\Phi = 10 \times 8$ mm, soldered on insulated copper wire and then protected by two-component epoxy resin, leaving a surface area of 0.5 cm² to contact the solution.

Investigations have been performed by open circuit measurements (E_{OC}) in time of 60 min, followed by electrochemical impedance measurements (EIS) at E_{OC} , from 50 kHz to 30 mHz frequency range, with 5 points per decade and a.c. *sinusoidal* potential *perturbation* (± 10 mV). After EIS measurements, the linear polarization method was performed in the potential region of ± 20 mV around E_{OC} , with the scanning rate (s.r.) of 0.2 mV s⁻¹, afterwards potentiodynamic polarization method in the potential region of -250 mV to 600 mV vs E_{OC} , with the s.r. = 0.5 mV s⁻¹. All electrochemical investigations were performed in triplicate. A

potentiostat/galvanostat (EG&G model 273A, USA) with EG&G M5210 lock-in amplifier were used. Measurements were performed in 0.5 M NaCl electrolyte with Pt-sheet auxiliary electrode and saturated calomel electrode (SCE) as the reference electrode. MetkonForcipol 1V grinder-polisher was used for mechanical treatment of electrodes with wet SiC emery papers (from 400 to 1500) and polishing with Al₂O₃ polishing suspension (0.05 μm) up to mirror finish. The electrode was then degreased in ethanol, washed in deionized water using Asonic ultrasonic cleaner, and then immersed in the electrolyte solution. Detailed surface analysis was performed with Scanning Electron Microscope Tescan Vega 5136 MM paired with Energy Dispersive Spectroscopy Microscopy (SEM/EDS).

3. RESULTS AND DISCUSSION

3.1. Hardness measurement

Average hardness values were calculated from three different measurements. Results are shown in Table 3.

Table 3 Hardness measurements of ADI samples

Wt. % Cu	Sample ID	Hardness HV10			
		Measurement 1	Measurement 2	Measurement 3	Average
0.32 %	10	279	268	272	273
	11	266	258	254	259
	12	455	421	433	436
	13	330	360	317	336
	14	294	294	330	306
	15	264	256	258	259
	16	279	232	228	246
0.91 %	20	270	306	312	296
	21	266	268	274	269
	22	266	274	287	276
	23	397	429	401	409
	24	327	351	351	343
	25	493	498	493	495
0.031 %	30	245	240	254	246
	31	333	330	325	329
	32	317	299	297	304
	33	238	232	233	234
	34	272	274	268	271
	35	330	333	325	329
0.51 %	40	272	272	266	270
	41	339	351	339	343
	42	249	251	247	249
	43	446	488	483	472
	44	446	442	455	448
	45	264	274	260	266

Fig. 1 shows the dependence of hardness on austempering temperature and time for each ADI alloy. The hardness decreases with increasing austempering temperature and time. Higher hardness at lower austempering temperatures and times relates to smaller amounts of carbon

enriched retained austenite and a larger amount of carbides, mainly silicon carbides that form simultaneously as ausferrite. Increasing of austempering temperatures and times, increases the volume fraction of retained austenite, which leads to a decrease in hardness, as seen in Fig. 1. Also, it is clear that hardness rises with the increase of copper content in the specimens. This is because, with larger amounts of copper in ductile iron samples, there is more perlite in starting microstructure which promotes carbide formation.

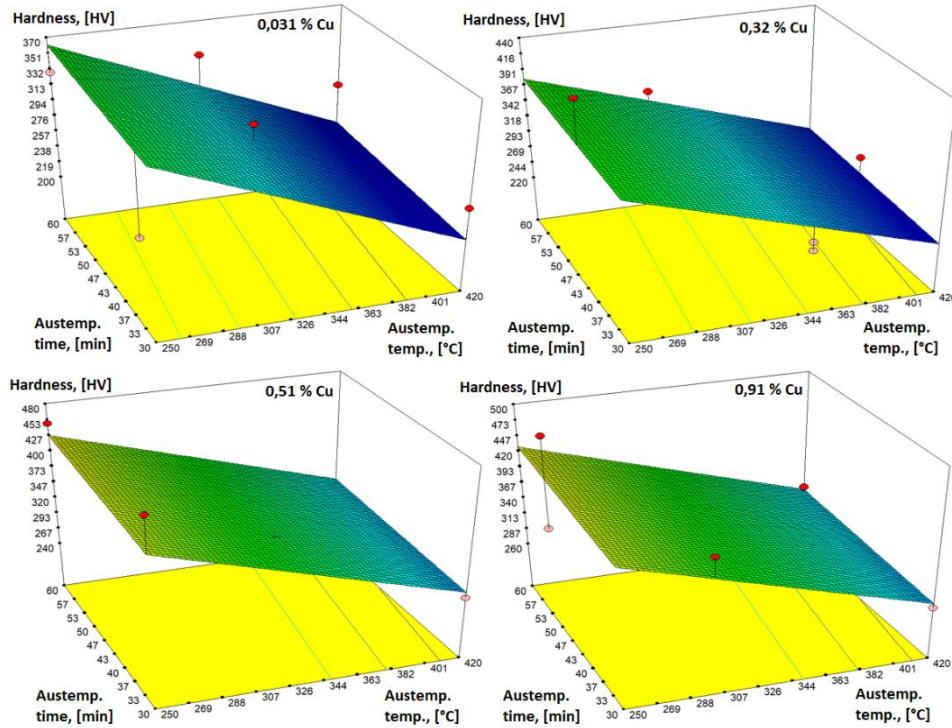


Fig. 1 Dependence of Vickers hardness HV10 on austempering temperature and time for each ADI alloy

The RSM analysis of measured hardness values for used experimental parameters yields an equation for each ADI alloy:

$$0.031 \% \text{ Cu:} \quad \text{HV} = 534.8 - 0.81154 \cdot T_a + 0.48636 \cdot \tau_a \quad (1)$$

$$0.32 \% \text{ Cu:} \quad \text{HV} = 552.02917 - 0.81154 \cdot T_a + 0.48636 \cdot \tau_a \quad (2)$$

$$0.51 \% \text{ Cu:} \quad \text{HV} = 602.07953 - 0.81154 \cdot T_a + 0.48636 \cdot \tau_a \quad (3)$$

$$0.91 \% \text{ Cu:} \quad \text{HV} = 603.64003 - 0.81154 \cdot T_a + 0.48636 \cdot \tau_a \quad (4)$$

The correlation coefficient of this fit is $r^2 = 0.6670$.

3.2. Electrochemical measurements

Fig. 2 a) illustrates the E_{OC} decay for DI samples in 0.5 M NaCl solution while Fig. 2 b) showed changes of E_{OC} for ADI with the lowest and the highest amount of Cu. The electrode potentials for all samples changed to negative values after immersion into the electrolyte solution due to the adsorption of chloride ions on the electrode surface, which trigger the corrosion processes on the surface of the alloy. Similar behavior for DI and ADI exposed to the chloride solution was established in the literature [18,19]. This change is most noticeable in the first 20 minutes of electrode immersion, after which potential changes with time become less pronounced and the stabilization of the open circuit potential values occurred. The final values of E_{OC} of all investigated samples do not differ significantly (potential differences are less than 20 mV).

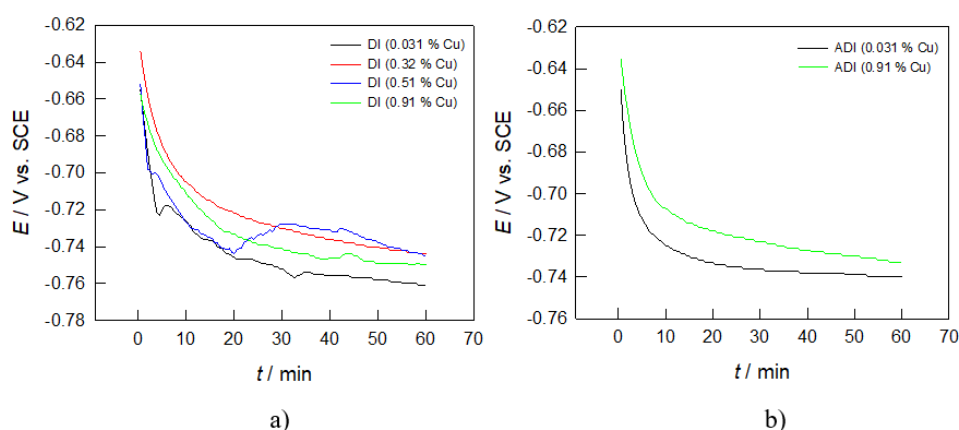


Fig. 2 Open circuit potential changes for a) ductile iron samples and b) austempered ductile iron samples in 0.5M NaCl solution at 20°C

Fig. 2 b) showed E_{OC} measurements of ADI samples with the highest and lowest Cu content (0.91% and 0.031%), which have a similar trend of lowering values of E_{OC} with time like DI samples. Slightly more negative values of E_{OC} have been observed for the ADI sample with the lowest percentage of Cu, and the final potential difference was around 20 mV. ADI samples showed more positive E_{OC} values than ductile iron samples with the same Cu composition, implying higher corrosion resistance than DI samples.

To obtain a physical image of the observed systems and explain the influence of Cu content on corrosion of DI and ADI at E_{OC} , impedance measurements have been performed, and the results are shown in Figs. 3 and 4 in the form of the Nyquist plot. Only one capacitive loop was observed, which described the dielectric properties of corrosion product film on DI surface [14,20,21]. The capacitive loop diameter increases with the Cu content of in alloy.

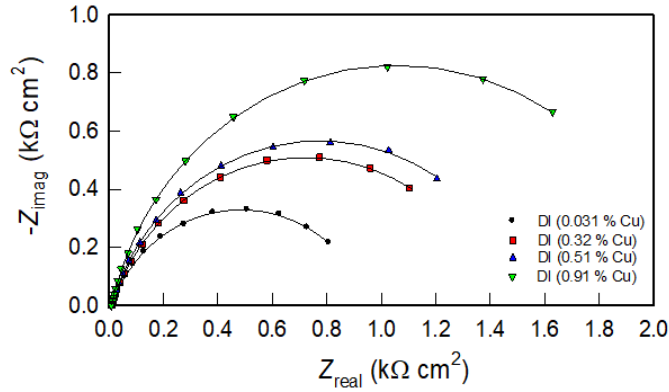


Fig. 3 Nyquist plots for ductile iron in 0.5 mol dm⁻³ NaCl solution

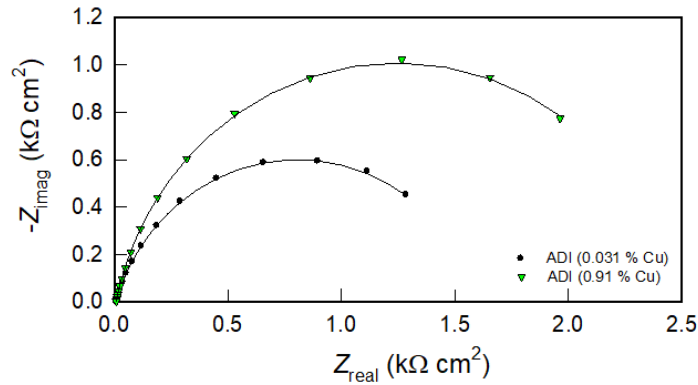


Fig. 4 Nyquist plots for austempered ductile iron in 0.5 mol dm⁻³ NaCl solution

Since the analysis of impedance measurements showed that the capacitive loops are flattened, a constant phase element (CPE) was used instead of an "ideal" capacitor. The impedance of CPE (Z_{CPE}) is given by the expression [22]:

$$Z_{CPE} = [Q(j\omega)^n]^{-1} \quad (5)$$

where constant Q accounts for a combination of properties related to both the surface and the electroactive species, $j\omega$ is the complex variable for sinusoidal perturbation with $\omega = 2\pi f$ and n is the exponent of CPE. Exponential term n can assume values from -1 to $+1$. When the value of n is close to 1, the CPE behaves like an ideal capacitance, while n values relative to 0.5 indicate diffusion processes. Consequently, the CPE represents a Warburg diffusion component. Furthermore, for n values close to 0, the CPE represents the resistance and inductance for n close to -1 .

The obtained spectra are accompanied by a simple equivalent circuit, shown in Fig. 5, which consist of R_{el} (electrolyte resistance), R (resistance) and Q (capacitance) of the surface corrosion product film, and the calculated values are presented in Table 4. According to the fitting results, the n values for Q are about 0.77-0.87. Hence, in the proposed

equivalent circuit, Q is a constant phase element (CPE) representing surface layer capacitances combined with diffusion processes.

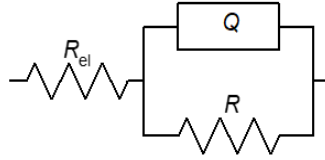


Fig. 5 Proposed equivalent circuits for modeling the impedance data

The addition of Cu increases the resistance and reduces the capacity which is connected to the better protective properties of the surface corrosion layer. Exponential term n also increases, indicating a reduced diffusion through the surface layer due to the increase in its compactness. The same effect was observed in the heat treatment of specific DI samples, i.e., samples with the lowest and highest Cu content (Fig. 4 and Table 4).

Table 4 Impedance parameters for DI and ADI in 0.5 M NaCl solution

Sample	DI		ADI			
% Cu	$Q_1 \times 10^3$ ($\Omega^{-1} s^n \text{cm}^{-2}$)	n_1	R_1 ($\text{k}\Omega \text{cm}^2$)	$Q_2 \times 10^3$ ($\Omega^{-1} s^n \text{cm}^{-2}$)	n_1	R_1 ($\text{k}\Omega \text{cm}^2$)
0.031	1.23	0.77	0.95	1.01	0.82	1.59
0.32	1.15	0.79	1.42	-	-	-
0.51	1.11	0.81	1.54	-	-	-
0.91	0.93	0.84	2.11	0.76	0.87	2.84

According to parallel *plate capacitor theory*, the surface film capacity, C , is inversely proportional to its thickness, d . Hence, the decrease of Q , with the increase of Cu content and heat treatment, leads to the corresponding increase in the thickness of the surface layer and additionally prevents iron corrosion at E_{OC} .

Alloying elements have a significant impact on the properties of the surface films. Thus, a better oxide film (with a more compact structure, higher resistance and thickness) will be formed on the alloy surface, which contains alloying elements that facilitate passivation, and this will be manifested with the increase in the corrosion resistance of the alloy, i.e., lower corrosion current and greater polarization resistance. According to literature, the 1 wt. % of copper addition effectively increased the retained austenite content, as copper can slow down stage II of bainitic transformation to offer a wider processing window, i.e., copper addition creates an increased range of austempering durations to obtain additional content of the retained austenite [23,24]. Furthermore, the addition of 1 wt. % Cu leads to a homogeneous distribution in microstructure regardless of as-cast and ADI, i.e., there was no copper-rich phase found in both the irons with copper addition [23].

The beneficial effect of Cu in DI and austempering heat treatment of sample on the corrosion resistance of the alloy (Table 1 and 2) could be explained as the copper addition reduced the number of the graphite nodules and thus alleviated graphite corrosion, while the austempering heat treatment allowed the formation of the retained austenite, which has an action like a corrosion inhibitor [23]. Graphite corrosion is a form of selective corrosion in

which graphite act as a strong cathode to iron and electrolytically accelerated the attack on the surrounding matrix [10,23]. Thus, experimental results indicated that the corrosive resistance of DI dependent on the number of graphite nodules in the microstructure and the retained austenite content in its microstructure. Therefore, it may be said that less nodule account and more retained austenite content could provide better corrosion resistance. This is also in accordance with the investigations of Seikh and associates [20], which observed that corrosion rate decrease linearly with the increasing volume fraction of retained austenite.

After EIS investigations, linear and potentiodynamic polarization measurements were conducted on the samples to determinate corrosion parameters such as values of polarization resistance (R_p), corrosion potentials (E_{corr}) and corrosion current densities (i_{corr}). Fig. 6 presents results of linear polarization measurements for the DI samples a) and potentiodynamic polarization curves b) in 0.5 M NaCl solution, while Fig. 7 presents results for ADI.

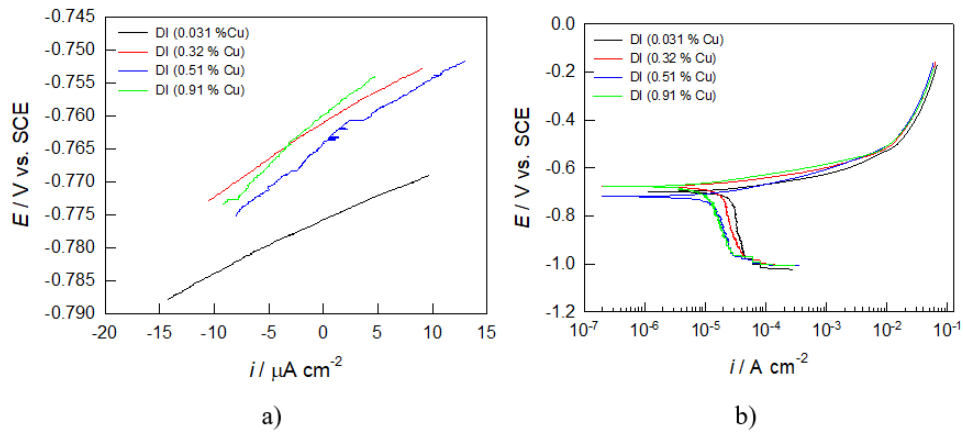


Fig. 6 Results of linear polarization measurements a) and potentiodynamic polarization measurements b) for ductile iron samples in 0.5M NaCl solution at 20°C

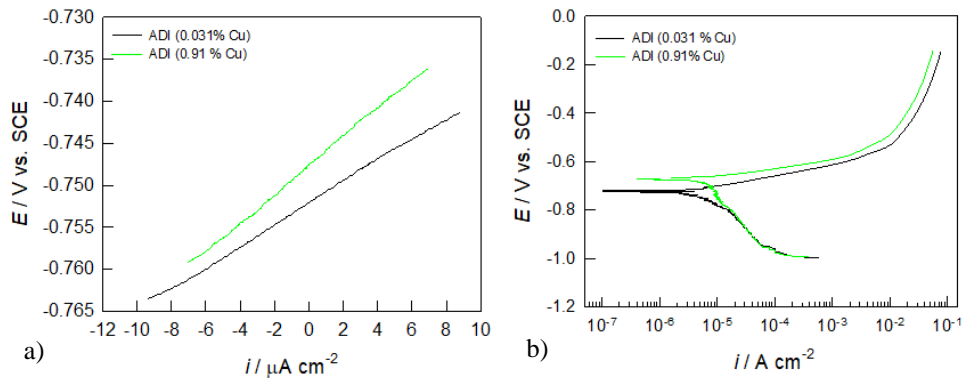


Fig. 7 Results of linear polarization measurements a) and potentiodynamic polarization measurements b) for austempered ductile iron samples in 0.5M NaCl solution at 20°C

In Figs. 6 a) and 7 a) it can be seen that the slope of the linear parts of the curves rises with the increase in the mass percentage of Cu in DI and ADI samples. The values of the polarization resistance, determined from the slopes of these linear parts, according to equation (5), are showed in Table 3. As R_p value is inversely proportional to the material corrosion rate, a higher R_p value corresponds to the higher corrosion resistance of alloy [23,26].

$$R_p = \frac{\Delta E}{\Delta i} \quad (6)$$

The results of potentiodynamic polarization measurements for DI in 0.5 M NaCl solution (Fig. 6 b)) show that increasing the percentage of Cu in the alloy leads to a decrease in anodic and cathodic current densities, which results in a lower value of corrosion current density. Therefore, it can be concluded that increasing Cu content in the alloy increases its corrosion resistance. ADI sample with higher Cu in the alloy shows lower anodic current densities and higher positive E_{corr} value than lower Cu ADI sample. The corrosion current density values for ADI samples have a significantly smaller difference with the alloy's copper content than ductile iron (Table 5).

Table 5 Corrosion parameters for DI and ADI in 0.5 M NaCl solution

Sample % Cu	DI			ADI		
	R_p ($k\Omega \text{ cm}^2$)	i_{corr} ($\mu\text{A cm}^{-2}$)	E_{corr} (V)	R_p ($k\Omega \text{ cm}^2$)	i_{corr} ($\mu\text{A cm}^{-2}$)	E_{corr} (V)
0.031	0.771	21.78	-0.693	1.275	6.96	-0.715
0.32	1.042	15.18	-0.676	-	-	-
0.51	1.115	11.67	-0.717	-	-	-
0.91	1.351	9.27	-0.670	1.710	6.34	-0.672

The higher corrosion resistance of ADI with a higher percentage of Cu could be attributed to the combinatory effect of copper addition which reduced the nodule count to mitigate graphite corrosion and austempering high treatment, which led to the formation of the retained austenite, which has a protective role in ADI structure [24].

3.3. Surface analysis

To get more insight into corrosion processes on DI and ADI samples in NaCl solution, SEM analysis were performed on corroded surfaces. Also, EDS analysis was performed on selected DI and ADI samples. After polarization investigation and prior surface analysis, electrodes were cleaned ultrasonically in deionized water and dried in a desiccator. Fig. 8 shows SEM micrographs of the surface.

There are notable differences in SEM micrographs between corrode DI and ADI. The cathodic graphite nodules are clearly seen in Figs. a) and b) and also severe corrosion of matrix around the nodules according to the reaction (7):



The intensity of corrosion leads to graphite nodules peeled off, and the round cavities remained on the sample surfaces. Along with graphite (galvanic corrosion), uniform corrosion is also present. In ADI, graphite corrosion still occurs to a lesser extent, while uniform corrosion was minimal due to the occurrence of retained austenite in the matrix [7,14].

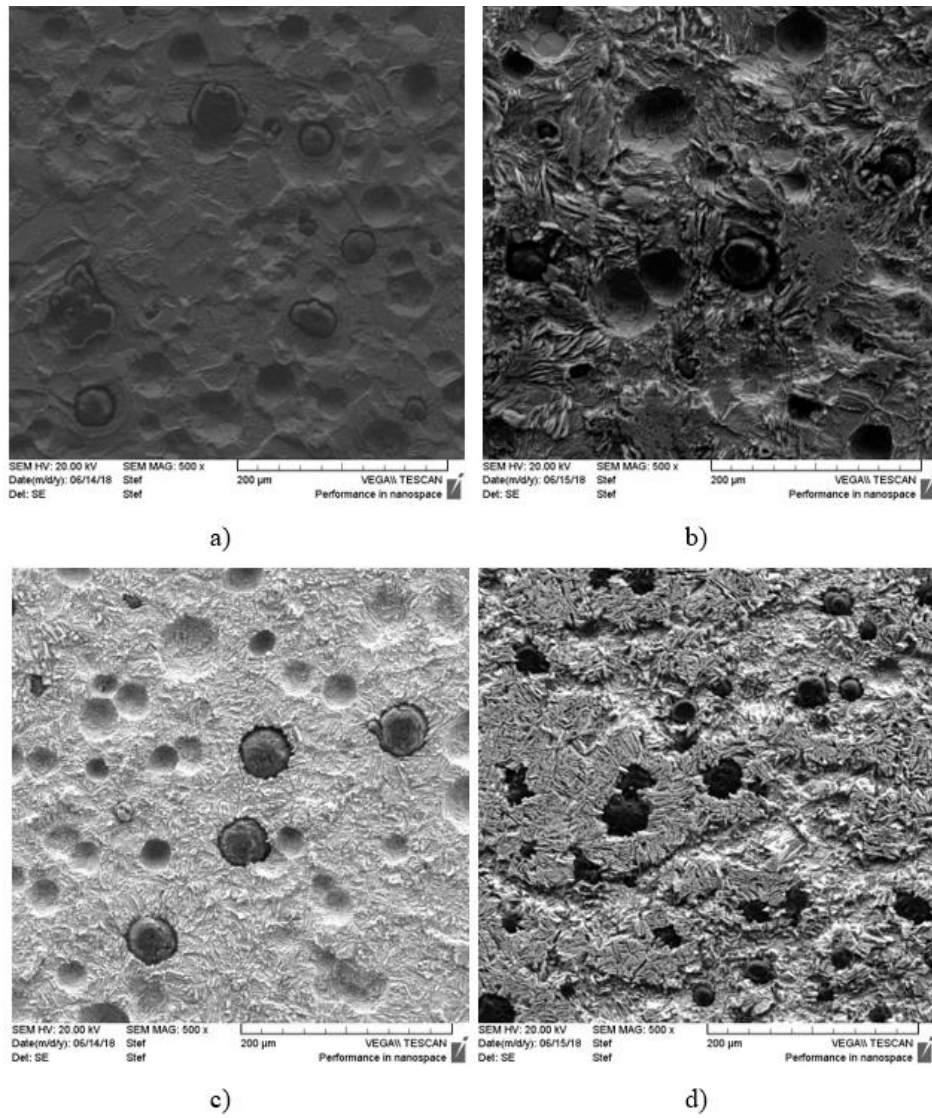


Fig. 8 SEM micrographs of DI with 0.031% Cu a) and 0.91% Cu b) and ADI with 0.031% Cu c) and 0.91% Cu d) after polarization measurements in 0.5 mol dm⁻³ NaCl solution

EDS analysis of the corroded DI sample with 0.91% Cu is presented in Fig. 9 and Table 6.

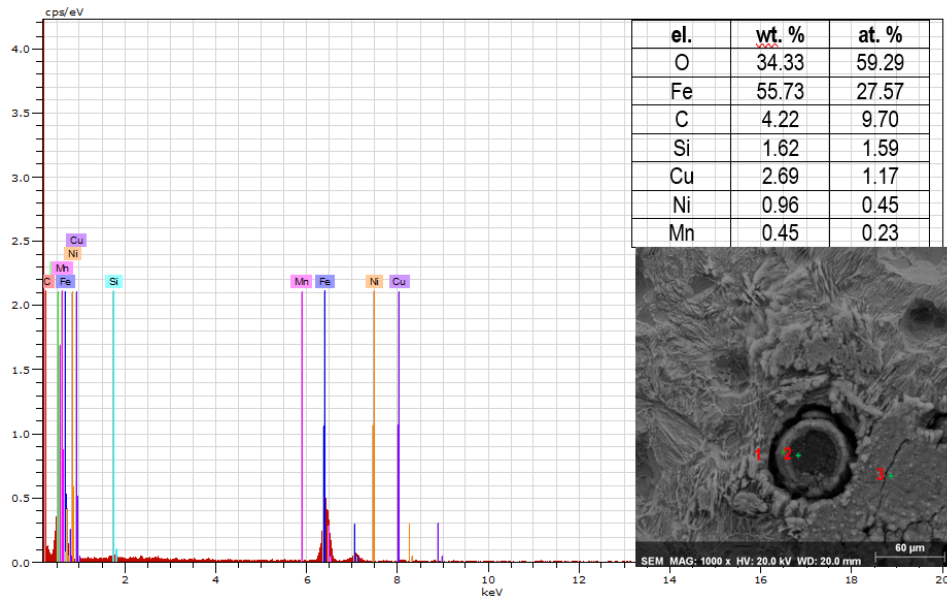


Fig. 9 EDS analysis of DI sample (3 different position): a) at the edge of graphite nodule, b) at the center of the graphite nodule, c) in the surrounding matrix

Table 6 EDS analysis of corroded DI sample for positions 2 and 3

Element	Position 2		Position 3	
	wt. %	at. %	wt. %	at. %
C	57.39	67.77	1.33	4.24
O	33.86	30.01	16.50	39.60
Fe	6.42	1.63	72.69	49.97
Cu	1.21	0.27	7.57	4.57
Ni	0.69	0.17	0.67	0.44
Si	0.17	0.09	0.47	0.64
Mn	0.27	0.07	0.78	0.54

EDS analysis was performed on the three positions on corroded DI surfaces. Position 1 was on the edge of the graphite nodule where dominant compounds were Fe and Cu oxides along with a small percentage of C, Si, Mn and Ni. The different composition was found at the center of the graphite nodule (Position 2), where dominant elements were C and O with the minor percentage of Fe, Cu, Si, Ni and Mn. Position 3 in the matrix around the nodule showed the dominant percentage of Fe and O with a relatively high percentage of Cu and C and a small percentage of other elements (Si, Mn and Ni).

EDS analysis of the corroded ADI sample with 0.91% Cu is presented in Fig. 10. and Table 7.

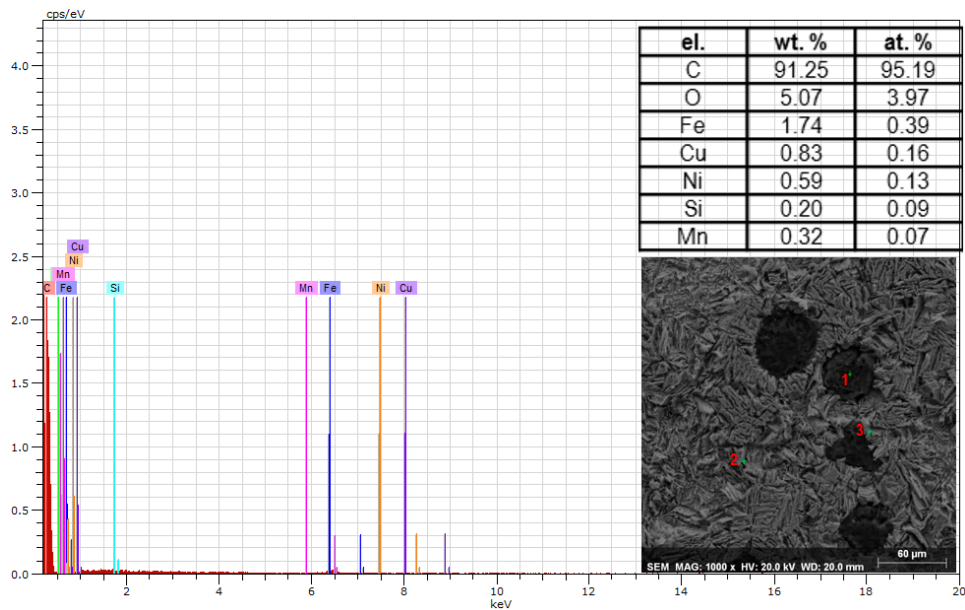


Fig. 10 EDS analysis of ADI sample (3 different positions): a) at the edge of graphite nodule, b) at the center of the graphite nodule, c) in the surrounding matrix

Table 7 EDS analysis of corroded ADI sample for positions 2 and 3

Element	Position 2		Position 3	
	wt. %	at. %	wt. %	at. %
Fe	83.72	63.48	85.09	65.74
O	7.72	20.44	5.54	14.93
C	2.94	10.38	4.07	14.63
Si	2.22	3.35	2.82	1.91
Cu	2.13	1.42	1.15	1.77
Ni	0.66	0.48	0.79	0.58
Mn	0.60	0.46	0.55	0.43

EDS analysis was performed on the three positions on corroded ADI surfaces. Position 1 was at the center of the nodule where the amount of C is dominant. All other elements are presented in low percentages. Position 2 was in the matrix, where a dominant element is Fe along with O and C, while the other elements are present in low percentage. The percentage of oxygen present in these two positions on the ADI surface is significantly smaller than a similar position on the DI surface. A similar composition in Position 2 has been found in Position 3, on the boundary between matrix and another partially deformed nodule. It should be noted that the content of carbon measurement with EDS is not accurate due to a low atomic number of carbon and hydrocarbon molecules on the surface.

4. CONCLUSION

In the present study, the influence of Cu content on hardness and corrosion properties of the DI and ADI in 0.5 M NaCl solution was investigated. Based on the experimentation and analyzing the results, the following conclusions can be drawn:

- The hardness decreases with increasing austempering temperature and time and rises with the increased copper content in the specimens.
- The beneficial effect of higher Cu content in DI and ADI towards corrosion resistance has been proved by polarization and EIS measurements. Higher polarization resistance and lower corrosion current density values for a higher percentage of Cu in DI and ADI and also increase in alloy surface resistance (R) and decrease in the surface layer capacity (Q) are connected to the better protective properties of the surface layer due to the increase in its compactness which indicates better corrosion resistance.
- Severe surface damages have been seen on DI samples due to the intensive galvanic corrosion resulting from the different potentials of graphite nodules and the surrounding matrix, along with the uniform corrosion attack. On the surface of ADI, graphite corrosion still occurs but to a lesser extent, while uniform corrosion was minimal due to retained austenite in the matrix.
- EDS analysis has shown that the around matrix has the highest content of iron and a higher percentage of alloying elements than the produced alloy before polarization measurements which refers to the intensive iron dissolution from the matrix, which increases the content of alloying elements on the surface.

REFERENCES

1. Davies, J.R., Davies & Associates, 2001, *Alloying: understanding the basics*, ASM International, Materials Park, Ohio, USA.
2. Janjić, M., Avdušinović, H., Jurković, Z., Bikić, F., Savičević, S., 2016, *Influence of austempering heat treatment on mechanical and corrosion properties of ductile iron samples*, *Metalurgija*, 55(3), pp. 325-328.
3. Sosa, A.D., Rosales, C.S., Boeri, R.E., Simison, S.N., 2016, *Corrosion mechanisms in ADI parts*, *International Journal of Cast Metals Research*, 29(1-2), pp. 105-110.
4. Hsu, C.-H., Lin, K.-T., 2011, *A study on microstructure and toughness of copper alloyed and austempered ductile irons*, *Materials Science and Engineering: A*, 528(18), pp. 5706-5712.
5. Harding, R.A., *The production, properties and automotive applications for austempered ductile iron*, *Metallic Materials*, 45(1), pp. 1-16.
6. Han, Ch.F., Wang, Q.Q., Sun, Y.F., Li, J., 2015, *Effects of molybdenum on wear resistance and corrosion resistance of carbidicaustempered ductile iron*, *Metallography, Microstructure and Analysis*, 4(4), pp. 298-304.
7. Čatipović, N., Živković, D., Dadić, Z., 2018, *The Effects of molybdenum and manganese on the mechanical properties of austempered ductile iron*, *Technical Gazette*, 25(2), pp. 635-642.
8. Labrecque, C., Gagne, M., *Ductile iron: fifty years of continuous development*, *Canadian Metallurgical Quarterly*, 37(5), pp. 343-378.
9. Francucci, G., Sikora, J., Dommarco, R., 2008, *Abrasion resistance of ductile iron austempered by the two-step process*, *Materials Science and Engineering: A*, 485(1-2), pp. 46-54.
10. Hsu, C.H., Chen, M.L., 2010, *Corrosion behavior of nickel alloyed and austempered ductile irons in 3.5% sodium chloride*, *Corrosion Science*, 52(9), pp. 2945-2949.
11. Hsu, C.H., Chen, M.L., Hu, C.J., 2007, *Microstructure and mechanical properties of 4% cobalt and nickel alloyed ductile irons*, *Materials Science and Engineering: A*, 444(1-2), pp. 339-346.
12. Čatipović, N., Živković, D., Dadić, Z., Ljumović, P., 2021, *Effect of copper and heat treatment on microstructure of austempered ductile iron*, *Transactions of the Indian Institute of Metals*, 74(6), pp. 1455-1468.

13. Afolabi, A.S., 2011, *Effect of austempering temperature and time on corrosion behavior of ductile iron in chloride and acidic media*, Anti-Corrosion Methods and Materials, 58(4), pp. 190-195.
14. Nofai, A.A., Ahmed, A.S.I., Ghanem, W.A., Hussein, W.A., El-dabaa N.K., 2019, *The effect of austempering heat treatments on the microstructure and corrosion behaviour of cast iron in 3.5% sodium chloride solutions*, International Journal of Advanced Research (IJAR), 7(4), pp. 1551-1558.
15. Zeng, D., Yung, K.C., Xie, C., 2001, *Investigation of corrosion behaviour of high nickel ductile iron by laser surface alloying with copper*, Scripta Materialia, 44(12), pp. 2747-2752.
16. Li, H.Z.J., Zhen, Z., Wang, A., Zeng, D., Miao, Y., 2016, *The microstructures and tribological properties of composite coatings formed via PTA surface alloying of copper on nodular cast iron*, Surface and Coatings Technology, 286, pp. 303-312.
17. Design Expert 7: DX7 Help – Backward Elimination Regression, State-Ease, 2005.
18. Igea, O.O., Olawale, O.J., Oluwasegun, K.M., Aribo, S., Obadele, B.A., Olubambi, P.A., 2017, *Corrosion behavior of austempered ductile iron produced by forced air quenching method in simulated mine water*, Procedia Manufacturing, 7, pp. 579-583.
19. Akinribide, O.J., Akinwamide, S.O., Ajibola, O.O., Obadele, B.A., Olusunle, S.O.O., Olubambi, P.A., 2019, *Corrosion behavior of ductile and austempered ductile cast iron in 0.01M and 0.05 M NaCl environments*, Procedia Manufacturing, 30, pp. 167-172.
20. Seikh, A.H., Sarkar, A., Singh, J.K., Mohammed, S.M. A.K., Alharthi, N., Ghosh, M., 2019, *Corrosion Characteristics of Copper-Added Austempered Gray Cast Iron (AGCI)*, Materials, 12, 503.
21. Shen, H.P., Cheng, X.Y., Li, H., Zhang, S.Y., Su, L.C., 2015, *Effect of copper alloy element on corrosion properties of high strength mooring chain steel*, HSLA Steels 2015, Microalloying 2015 & Offshore Engineering Steels 2015, 1201.
22. Brett, C.M., Brett, A.M.O., 1993, *Electrochemistry principles, methods and applications, Chapter 11: Impedance methods*, Oxford University Press, Oxford, UK, pp. 224-251.
23. Hsu, C.H., Lin, K.T., 2014, *Effect of copper and austempering on corrosion behavior of ductile iron in 3.5 pct sodium chloride*, Metallurgical and Materials Transaction A, 45A(3), pp. 1517-1523.
24. Krishnaraj, D., Narasimhan, H.N.L., Seshan, S., 1992, *Structure and properties of ADI as affected by low alloy additions*, AFS Transactions 100, pp. 105-112.
25. Walton, C.F., 1981, *Iron Casting Handbook*, Iron Casting Society, Cleveland, Ohio, USA.
26. Argade, G.R., Panigrahi, S.K., Mishra, R.S., 2012, *Effects of grain size on the corrosion resistance of wrought magnesium alloys containing neodymium*, Corrosion Science, 58, pp. 145-151.